Electric circuit simulations of nth-Chern-number insulators in 2n-dimensional space and their non-Hermitian generalizations for arbitrary n

Motohiko Ezawa

Phys. Rev. B **100**, 075423 — Published 16 August 2019

DOI: 10.1103/PhysRevB.100.075423

Electric circuit simulations of nth-Chern insulators in $2n$-dimensional space and their non-Hermitian generalizations for arbitral n

Motohiko Ezawa
Department of Applied Physics, University of Tokyo, Hongo 7-3-1, 113-8656, Japan

We show that topological phases of the Dirac system in arbitral even dimensional space are simulated by LC electric circuits with operational amplifiers. The lattice Hamiltonian for the hypercubic lattice in $2n$ dimensional space is characterized by the n-th Chern number. The boundary state is described by the Weyl theory in $2n-1$ dimensional space. They are well observed by measuring the admittance spectrum. The results are extended to non-Hermitian systems with complex Dirac masses. The non-Hermitian n-th Chern number remains to be quantized for the complex Dirac mass.

I. INTRODUCTION

Topological insulators were originally discovered in condensed matter physics. Now the notion has been extended to cold atoms[1], photonics[2,3] and acoustics[4–7]. A recent finding is that it is also applicable to electric circuits[8,9]. Various topological phases have been simulated by electric circuits[8–18]. In this context, non-Hermitian topological systems are among hottest topics of artificial topological systems[16,19–25]. Nevertheless, all these phases are also realizable in condensed matter in principle. It is an interesting problem to explore exotic topological phases which would never exist in condensed matter.

An obvious example is the topological phase in the spatial d dimensions (dDs) with $d \geq 4$. The four-dimensional (4D) quantum Hall effect is one of them[26]. It is simulated via 2D quasi-crystals[27] or topological pumping in photonic systems[28–30] and optical lattices[31,32]. They are characterized by the second-Chern number. In the same way, the 6D quantum Hall effect is realized in 3D topological pumping[33,34].

In this paper, we show that topological phases of the Dirac system in any even dimensional space are simulated by LC electric circuits with operational amplifiers. Especially, we construct topological phases characterized by the n-th Chern number in $2n$Ds for arbitral n. We start with the Dirac Hamiltonian defined on the hypercubic lattice. The n-th Chern number is analytically calculated since it is determined by the Dirac theory at the 2^{2n} high-symmetry points. Then we show that the boundary states are described by the Weyl theory in (2n-1)D. They are manifested by calculating the density of states (DOS), which is proportional to $|E|^{2n-2}$. Finally, we point out that they are well signaled by admittance spectrum.

II. MODEL HAMILTONIAN

The Dirac Hamiltonian in $2n$D space is given by

$$H_{2n} = \int d^{2n}k \left[\psi^\dagger(k)\,\Gamma_j k_j \psi(k) + M\psi^\dagger(k)\,\Gamma_0\psi(k)\right], \tag{1}$$

where Γ_μ with $j = 1, 2, \cdots, 2n$ and $\mu = 0, 1, 2, \cdots, 2n$ are the gamma matrices satisfying the Clifford algebra $\{\Gamma_\mu, \Gamma_\nu\} = 2\delta_{\mu\nu} I$, while M is a constant representing the Dirac mass. The system becomes non-Hermitian when the mass M is taken to be complex. All the analysis is valid both for Hermitian and non-Hermitian systems.

The gamma matrix Γ_μ^{2n} in $2n$Ds has a 2^n dimensional representation, which is recursively defined by

$$\begin{aligned} \Gamma_0^{2n} &= \sigma_x \otimes \mathbb{I}^{2n-2}, \quad \Gamma_{2n}^{2n} = \sigma_z \otimes \mathbb{I}^{2n-2}, \\ \Gamma_j^{2n} &= \sigma_y \otimes \Gamma_j^{2n-2}, \quad \Gamma_{2n-1}^{2n} = \sigma_z \otimes \Gamma_0^{2n-2} \end{aligned} \tag{2}$$

for $1 \leq j \leq 2n-2$, and $\Gamma_0^2 = \sigma_z$, $\Gamma_1^2 = \sigma_x$, $\Gamma_2^2 = \sigma_y$.

The corresponding lattice model is[35,36],

$$H_{2n}(k) = \sum_{\mu=0}^{2n} \psi^\dagger(k)\, d^\mu \Gamma_\mu \psi(k), \tag{3}$$

where

$$d^0 = m + t\sum_{j=1}^{2n} \cos k_j, \qquad d^j = \lambda \sin k_j, \tag{4}$$

with the on-site potential m, the hopping amplitude t and the spin-orbital interaction λ. The energy spectrum is given by $E = \pm\sqrt{\sum_{\mu=0}^{2n} (d^\mu)^2}$.

First, we show the bulk DOS of the Hermitian system in Fig.1(a1)-(c1). The system is an insulator due to a finite gap.

Next, we show the energy spectrum in the ReE-ImE plane[37] for the non-Hermitian system in Fig.2(a1)-(c1). The two bulk spectra are separated by a line given by Re$E = 0$. This structure is called a line gap[38] charactering an insulator in the non-Hermitian system. It is a generalization of a point gap charactering an insulator in the Hermitian system.

The gap closes at the 2^{2n} high-symmetry points $\boldsymbol{K} = (K_1, K_2, \cdots, K_{2n})$, where $K_j = 0, \pi$. By evaluating (4) at these points, we obtain a set of 2^{2n} Dirac Hamiltonians (3) together with

$$d^0 = m + t\sum_{j=1}^{2n} (-1)^{K_j/\pi} \equiv \bar{m}, \quad d^j = (-1)^{K_j/\pi} \lambda k_j, \tag{5}$$

where d^0 is the Dirac mass at the point $\boldsymbol{K}$. We define the sign of the Dirac Hamiltonian by $\eta(\boldsymbol{K}) \equiv (-1)^{\sum K_j/\pi} = \pm 1$.

III. NON-HERMITIAN n-TH CHERN NUMBER

The topological insulator without any symmetry is classified by the $\mathbb{Z}$ index for both of the Hermitian[39,40] and non-

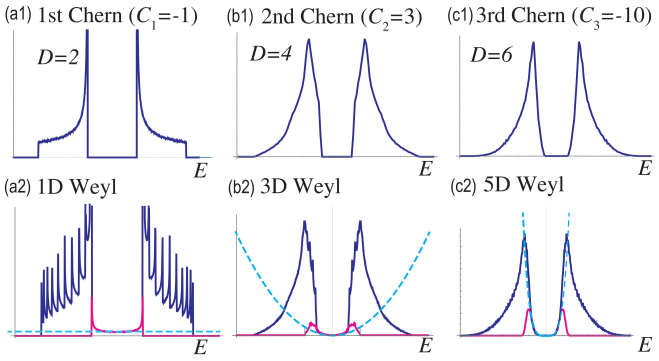

FIG. 1: (a1)–(c1) DOS of the bulk in n-th Chern insulators for the Hermitian system as a function of the energy E for (a) $D = 2$ with $C_1 = -1$, (b) $D = 4$ with $C_2 = 3$, and (c) $D = 6$ with $C_3 = -10$. There are finite gaps, dictating that the systems are insulators. (a2)–(c2) DOS of the boundary states as a function of the energy E. The dark blue curves represent the DOS for all bands numerically obtained, the magenta curves represent the DOS for the energy (14) analytically obtained, and the dotted cyan curves represent the DOS for the energy (15) analytically obtained. These numerical results are well fitted by analytical results of the Weyl theory in the vicinity of the Fermi energy. We have set $t = \lambda = m = 1$.

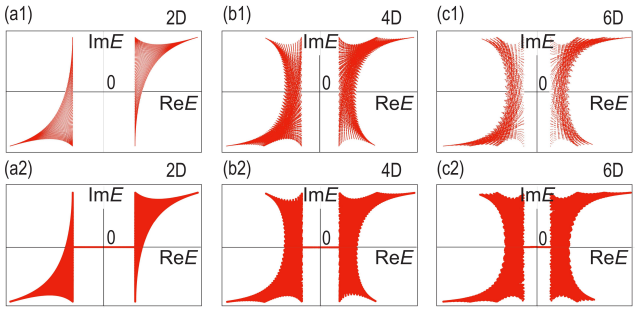

FIG. 2: Energy spectrum in the ReE-ImE plane for (a) $D = 2$ ($L = 100$), (b) $D = 4$ ($L = 25$) and (c) $D = 6$ ($L = 25$), where L is the length of the hypercube. (a1)–(c1) There are gaps in the bulk spectrum, showing that the system is an insulator. (a2)–(2) There are boundary states connecting two bulk spectra, which is on the Im$E = 0$ line. They are Weyl boundary states. We have set $t = \lambda = 1$ and $m = 1 + 0.1i$.

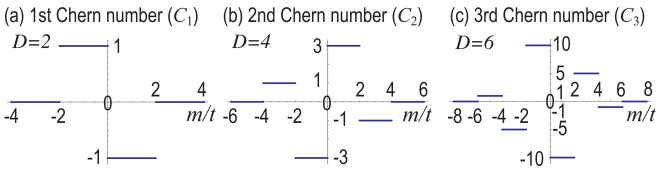

FIG. 3: n-th Chern number as a function of m for (a) $D = 2$, (b) $D = 4$ and (c) $D = 6$. We have set $\lambda = 1$.

Hermitian systems[38]. In the case of the Hermitian system, the topological number is the n-th Chern number. It is also applicable to the non-Hermitian system by using the following definition.

By generalizing the non-Hermitian Chern number[17,37,41–46], we define the non-Hermitian n-th Chern number as

$$C_n = \frac{1}{(2\pi)^n} \int \frac{1}{n!} \bigwedge^n F d^{2n}k, \tag{6}$$

where F is the non-Hermitian non-Abelian Berry curvature,

$$F_{ij}^{\alpha\beta} = \partial_i A_j^{\alpha\beta} - \partial_j A_i^{\alpha\beta} + i\left[A_i, A_j\right]^{\alpha\beta}, \tag{7}$$

with the non-Hermitian Berry connection[41,47–49]

$$A_i^{\alpha\beta}(k) = -i\langle\psi_\alpha^{\mathrm{L}}(k)|\partial_{k_i}|\psi_\beta^{\mathrm{R}}(k)\rangle. \tag{8}$$

Here, $|\psi_\beta^{\mathrm{R}}(k)\rangle$ and $|\psi_\beta^{\mathrm{L}}(k)\rangle$ are the right and left eigenstates, $H|\psi_\beta^{\mathrm{R}}(k)\rangle = E|\psi_\beta^{\mathrm{R}}(k)\rangle$ and $H^\dagger|\psi_\beta^{\mathrm{L}}(k)\rangle = E^*|\psi_\beta^{\mathrm{L}}(k)\rangle$.

Substituting (5) into (6), the n-th Chern number is given by

$$C_n(K_\mu) = \eta \frac{(4n-1)!!}{2^{n-1}(2n-1)!} \int d^{2n}k \frac{\bar{m}}{\left(k^2+\bar{m}^2\right)^{(2n+1)/2}}, \tag{9}$$

which is explicitly calculated as

$$C_n(K_\mu) = \eta \frac{\bar{m}}{2\sqrt{\bar{m}^2}}. \tag{10}$$

It reads $C_n(K_\mu) = \eta/2$ for $\mathrm{Re}[\bar{m}] > 0$ and $C_n(K_\mu) = -\eta/2$ for $\mathrm{Re}[\bar{m}] < 0$. It is quantized even for a complex mass.

The topological phase boundaries are determined by the massless condition $\bar{m}(K_\mu) = 0$, which is independent of the value of the spin-orbital interaction λ.

Then the total n-th Chern number for the lattice Hamiltonian is $C_n = \sum_{K_j} C_n(K_j)$, where the summation is taken over all the highest symmetry points. We show the n-th Chern number as a function of m/t in Fig.3. It is always quantized and jumps when the mass becomes zero.

IV. WEYL BOUNDARY STATES

The boundary states emerge in a topological phase of an insulator. Let us review the case of 2Ds, where we analyze a nanoribbon with a finite width along the x_2 axis. First of all, the dynamical degree of freedom with respect to x_2 is frozen by the Jackiw-Rebbi solution of the Dirac equation[50], where the mass has a spatial dependence. On the other hand, the lattice structure along the x_1 axis allows us to introduce the crystal momentum k_1. Consequently, the dynamical degree of freedom is carried solely by the momentum k_1 along the edge.

Similarly in $2n$Ds, we analyze a nanostructure with a finite thickness along the x_{2n} axis, while the other directions are periodic. We numerically calculate the energy spectrum of the non-Hermitian system in the ReE-ImE plane as in Fig.2(a2)–(c2). There are lines connecting two separated bulk spectra along the Im$E = 0$ line in topological phases. They are Weyl boundary states, which remains to be real even for the non-Hermitian system. It results in the emergence of a zero-energy solution, which is the Jackiw-Rebbi solution as we now demonstrate.

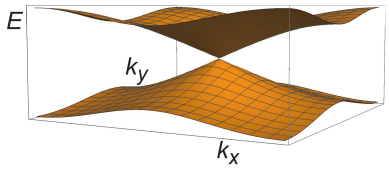

FIG. 4: Cone structure of the Weyl boundary state. The vertical axis is E, while the horizontal axes are k_x and k_y. We have set the other momenta are zero, $k_j = 0$ for $3 \leq j \leq 2n-1$. It does not depend on the dimension. The parameters are the same as Fig.2.

The Dirac equation describing the boundary states is given by

$$(\bar{m}\left(x_{2n}\right)\sigma_x \otimes \mathbb{I}^{2n-2} - i\lambda\partial_{x_{2n}}\sigma_y \otimes \mathbb{I}^{2n-2} + \sum_{j=1}^{2n-1} k_j\sigma_z \otimes \Gamma_{j-1})\psi = 0, \quad (11)$$

where $\bar{m}\left(x_{2n}\right)$ is a spatially dependent mass, $\bar{m}\left(x_{2n}\right) = m_0 \tanh(x_{2n}/\xi)$, with ξ the penetration depth. We seek a zero-energy solution by solving

$$\begin{pmatrix} 0 & \bar{m}\left(x_{2n}\right) - \lambda\partial_{x_{2n}} \\ \bar{m}\left(x_{2n}\right) + \lambda\partial_{x_{2n}} & 0 \end{pmatrix}\begin{pmatrix} \psi_A \\ \psi_B \end{pmatrix} = 0, \quad (12)$$

and find that $\psi_{A(B)} \propto \exp[\mp\lambda^{-1}\int \bar{m}\left(x_{2n}\right)dx_{2n}]$. This is exactly the Jackiw-Rebbi solution. The zero-energy solutions exist when the integrands converge. We have obtained the Jackiw-Rebbi solution even in the non-Hermitian system.

Since the dynamical degree of freedom with respect to x_{2n} is frozen, the dimensional reduction occurs from $2n$Ds to $(2n-1)$Ds, where the dynamical degrees of freedom are crystal momenta k_j with $1 \leq j \leq 2n-1$. The zero-energy solution is localized at the boundary, where the mass becomes zero. Hence, the boundary Hamiltonian is described by the Weyl Hamiltonian in $(2n-1)$Ds,

$$H_{2n-1}\left(k\right) = \sum_{j=1}^{2n-1} \psi^{\dagger}\left(k\right) d^j \Gamma_j \psi\left(k\right), \quad (13)$$

whose energy spectrum is given by

$$E\left(k\right) = \pm\left|\lambda\right|\sqrt{\sum_{j=1}^{2n-1}\sin^2 k_j}. \quad (14)$$

The energy dispersion is linear near the Fermi level,

$$E\left(k\right) = \pm\left|\lambda k\right|. \quad (15)$$

We show the boundary states numerically obtained as a function of k_x and k_y for the n-th Chern insulator based on the Hamiltonian (3) in Fig.4, where we have set $k_j = 0$ for $3 \leq j \leq 2n-1$. It is well fitted by (14).

The DOS is

$$\rho\left(E\right) = \int \delta(E - \lambda\sqrt{\sum_{j=1}^{2n-1}\sin^2 k_j})d^{2n-1}k, \quad (16)$$

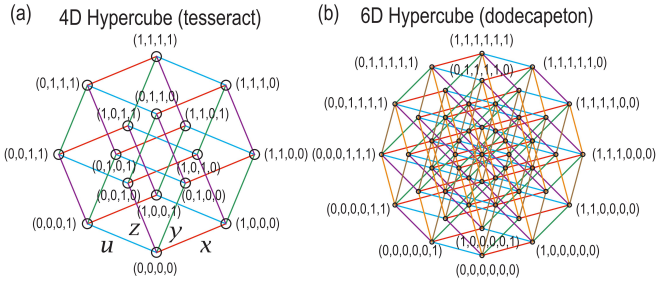

FIG. 5: Projection of the unit hypercube onto the 2D plane. (a) 4D hypercube and (b) 6D hypercube. Circles represent the unit cell shown in Fig.6, and colored links represent the conection between two unit cells as in Fig.6. The coordinates are shown in (a) and (b).

which is proportional to

$$\rho\left(E\right) \propto \lambda\left|E\right|^{2n-2} \quad (17)$$

in the vicinity of the Fermi level.

We numerically calculate the DOS of the thin film in the case of the Hermitian system in Fig.1(a2)-(c2). In the vicinity of the Fermi level, the DOS of the total band is well fitted by the DOS determined by the boundary lattice Hamiltonian (14) and the DOS (17) of the Weyl Hamiltonian. The DOS of the Hamiltonian is observable by measuring admittance, as we shall see later. Thus, it is an experimental signature to detect higher-dimensional Weyl boundary states.

V. ELECTRIC CIRCUIT REALIZATION

We next explain how to simulate the above model in higher dimensions by electric circuits. First, we note that a hypercubic lattice in any dimensions can be projected to a 2D plane as illustrated in Fig.5. The lattice points of a hypercube are projected to different positions in the 2D plane. Although the links cross each other, they can be avoided by using a bridge structure of wiring. We consider a hypercubic lattice structure in $2n$Ds whose unit cell contains 2^{2n} sites, which is the dimension of the Γ matrix.

Let us explain an instance of the 4D lattice, i.e., the case of $n = 2$. A single cube ($L = 1$) contains 16 sites as in Fig.5(a1). A pair of two sites are connected by a colored link, which is parallel to one of the four axes, i.e., the x-axis (red), the y-axis (green), the z-axis (purple) and the u-axis (cyan). A lattice with size $L = 3$ is illustrated in Fig.5(a2), which is obtained by dividing an edge of a single cube into $L = 3$ pieces.

Second, we associate one unit cell with each site, and one link circuit with each link: There are four types of link circuits in 4D lattice as illustrated in Fig.6. Actual forms of the unit cell and the link circuits are constructed by analyzing the Kirchhoff current law.

The Kirchhoff current law of the circuit under the application of an AC voltage $V\left(t\right) = V\left(0\right)e^{i\omega t}$ is given by[8,9],

$$I_a\left(\omega\right) = \sum_b \mathcal{J}_{ab}\left(\omega\right)V_b\left(\omega\right), \quad (18)$$

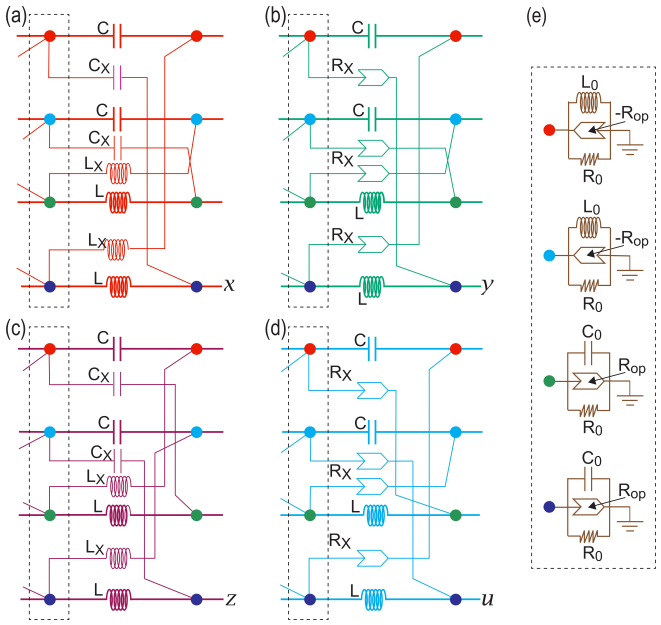

FIG. 6: Basic elements for electric circuit realization of the second-Chern insulator on the 4D hypercubic lattice. The dotted rectangle represents the unit cell. Colored circuits in (a) red, (b) green, (c) purple and (d) cyan represent links parallel to four independent axes x, y, z and u, respectively. (e) Each node is grounded either by a capacitance (C_0) or an inductor (L_0), together with an operational amplifier[14] ($R_{\rm op}$) and a resistor (R_0). The resister (R_0) is added in order to make the system stable. See also Fig.5 how to construct a whole circuit using the unit cell and links.

where the sum is taken over all adjacent nodes b, and $\mathcal{J}_{ab}(\omega)$ is called the circuit Laplacian. The eigenvalues of the circuit Laplacian are called the admittance spectrum, which provides us with an information of the bulk spectrum of the corresponding Hamiltonian.

We explain the method to implement an electric circuit corresponding to the Hamiltonian. The Hamiltonian is written in the form of the $2n \times 2n$ matrix. Each component has the form of $e^{\pm ik_\mu}$, $-e^{\pm ik_\mu}$or $ie^{\pm ik_\mu}$. We express the term $e^{\pm ik_\mu}$ by capacitors $i\omega C e^{\pm ik_\mu}$, the term $-e^{\pm ik_\mu}$ by inductors $-\frac{1}{i\omega L}e^{\pm ik_\mu}$, and the term $ie^{\pm ik_\mu}$ by operational amplifiers $iR_X e^{\pm ik_\mu}$ as in the case of the previous studies[8–14,17,18]. We introduce operational amplifiers $R_{\rm op}$ in order to make the Dirac mass complex. Then we connect each node either by a capacitor C_0 or an inductor L_0 to the ground as in Fig.6(e). The addition of operational amplifiers $R_{\rm op}$ may make the system unstable due to the gain induced by them. We can overcome the problem by introduding resistors R_0 parallel to them as in Fig.6(e). By using appropriate resistors, we can tune the system so that the gain is cancelled. For illustration in Fig.2 we have neglected the effect of resistors R_0 since they only shift the energy.

Let us explicitly show the implementation in the case of 4Ds. In order to make a circuit simple, we take a representation $\Gamma^0 = \sigma_z \otimes I$, $\Gamma^x = \sigma_x \otimes \sigma_x$, $\Gamma^y = \sigma_x \otimes \sigma_y$, $\Gamma^z = \sigma_x \otimes \sigma_z$ and $\Gamma^u = \sigma_y \otimes I$ for the second-Chern insulator. We show the element of the circuit structure in Fig.6. We use these structures colored in red, green, purple and cyan as x, y, z and u links in Fig.5, while the unit cell is denoted by black dotted rectangles.

It is straightforward to write down the circuit Laplacian[51] $\mathcal{J}_{ab}$ explicitly in terms of the capacitors, the inductors and the operational amplifiers used in the circuit given in Fig.6. Then, we fix these parameters in electric circuit so that the circuit Laplacian $\mathcal{J}$ is identical to the Hamiltonian H. It follows that $\mathcal{J} = i\omega H$, provided the resonance frequency is given by $\omega_0 = 1/\sqrt{LC} = 1/\sqrt{L_0 C_0}$. The relations between the system parameters are $t = C$, $\lambda = C_X = (\omega_0 R_X)^{-1}$, and $m = -4nC + C_0 - (i\omega R_{\rm op})^{-1}$. An important observation is that we may change the mass m by tuning C_0. Then, we may induce topological phase transitions by controlling the Chern number based on the formula (10) together with (5).

We present an explicit form of the circuit Laplacian corresponding to the circuit in Fig.6 in the main text. It is a sum of five terms in 4Ds, $\mathcal{J} = \sum_{\mu=0,x,y,z,u} \mathcal{J}_\mu$, with

$$\mathcal{J}_0 = \frac{1}{i\omega R_0} + \begin{pmatrix} m^+ & 0 & 0 & 0 \\ 0 & m^+ & 0 & 0 \\ 0 & 0 & m^- & 0 \\ 0 & 0 & 0 & m^- \end{pmatrix}, \tag{19}$$

$$\mathcal{J}_x = \begin{pmatrix} f_x^+ & 0 & 0 & g_x^0 \\ 0 & f_x^+ & g_x^0 & 0 \\ 0 & g_x^0 & f_x^- & 0 \\ g_x^0 & 0 & 0 & f_x^- \end{pmatrix}, \tag{20}$$

$$\mathcal{J}_y = \begin{pmatrix} f_y^+ & 0 & 0 & g_y^- \\ 0 & f_y^+ & g_y^+ & 0 \\ 0 & g_y^- & f_y^- & 0 \\ g_y^+ & 0 & 0 & f_y^- \end{pmatrix}, \tag{21}$$

$$\mathcal{J}_z = \begin{pmatrix} f_z^+ & 0 & g_z^0 & 0 \\ 0 & f_z^+ & 0 & -g_z^0 \\ g_z^0 & 0 & f_z^- & 0 \\ 0 & -g_z^0 & 0 & f_z^- \end{pmatrix}, \tag{22}$$

$$\mathcal{J}_u = \begin{pmatrix} f_u^+ & 0 & g_u^- & 0 \\ 0 & f_u^+ & 0 & g_u^- \\ g_u^+ & 0 & f_u^- & 0 \\ 0 & g_u^+ & 0 & f_u^- \end{pmatrix} \tag{23}$$

with

$$m^+ = C_0 - (i\omega R_{\rm op})^{-1}, \tag{24}$$

$$m^- = -(\omega^2 L_0)^{-1} + (i\omega R_{\rm op})^{-1}, \tag{25}$$

$$f_j^+ = 2C\cos k_j - 2C, \tag{26}$$

$$f_j^- = -2(\omega^2 L)^{-1}\cos k_j + 2(\omega^2 L)^{-1}, \tag{27}$$

$$g_j^+ = -(\omega^2 L_X)^{-1} e^{ik_j} + C_X e^{-ik_j}, \tag{28}$$

$$g_j^- = C_X e^{ik_j} - (\omega^2 L_X)^{-1} e^{-ik_j}, \tag{29}$$

$$g_j^0 = (i\omega R_X)^{-1} e^{ik_j} - (i\omega R_X)^{-1} e^{-ik_j}. \tag{30}$$

The system becomes an LC resonator.

The eigenvalues of the circuit Laplacian give an admittance spectrum[8–13]. Indeed the band structure of the circuit Laplacian can be experimentally observed[11] directly. Then, the DOS of the Laplacian is proportional to the DOS of the

Hamiltonian. Thus, the DOS of the Laplacian is measured by the DOS of the admittance by integrating out the momentum.

VI. DISCUSSIONS

We have shown that topological insulators in any dimensions are simulated by electric circuits. In elementary particle physics, the spatial dimension is believed to be higher than three according to string theory. On the other hand, the classification table of the topological insulator dictates the existence of the topological systems in higher dimensions[38–40]. However, these higher dimensional systems are impossible to approach experimentally. Our results will open a rout to study higher dimensional physics in laboratory.

The author is very much grateful to N. Nagaosa for helpful discussions on the subject. This work is supported by the Grants-in-Aid for Scientific Research from MEXT KAKENHI (Grants No. JP17K05490, No. JP15H05854 and No. JP18H03676). This work is also supported by CREST, JST (JPMJCR16F1 and JPMJCR1874).

[1] N. Goldman, J. C. Budich, P. Zoller, Nat. Phys. 12, 639 (2016).
[2] L. Lu, J. D. Joannopoulos and M. Soljačić, Nature Photonics 8, 821 (2014)
[3] T. Ozawa, H. M. Price, A. Amo, N. Goldman, M. Hafezi, L. Lu, M. C. Rechtsman, D. Schuster, J. Simon, O. Zilberberg, and I. Carusotto Rev. Mod. Phys. 91, 015006 (2019)
[4] Z. Yang, F. Gao, X. Shi, X. Lin, Z. Gao, Y. Chong, B. Zhang, Phys. Rev. Lett. 114, 114301 (2015)
[5] H. Xue, Y. Yang, F. Gao, Y. Chong and B. Zhang, Nature Materials 18, 108 (2019).
[6] X. Ni, M. Weiner, A. Alu, and A. B. Khanikaev, Nature Materials 18, 113 (2019).
[7] W. Zhu, X. Fang, D. Li, Y. Sun, Y. Li, Y. Jing and H. Chen, Phys. Rev. Lett. 121, 124501 (2018)
[8] C. H. Lee , S. Imhof, C. Berger, F. Bayer, J. Brehm, L. W. Molenkamp, T. Kiessling and R. Thomale, Communications Physics, 1, 39 (2018).
[9] S. Imhof, C. Berger, F. Bayer, J. Brehm, L. Molenkamp, T. Kiessling, F. Schindler, C. H. Lee, M. Greiter, T. Neupert, R. Thomale, Nat. Phys. 14, 925 (2018).
[10] M. Serra-Garcia, R. Susstrunk and S. D. Huber, Phys. Rev. B 99, 020304 (2019).
[11] T. Helbig, T. Hofmann, C. H. Lee, R. Thomale, S. Imhof, L. W. Molenkamp and T. Kiessling, Phys. Rev. B 99, 161114(R) (2019).
[12] Y. Lu, N. Jia, L. Su, C. Owens, G. Juzeliunas, D. I. Schuster and J. Simon, Phys. Rev. B 99, 020302 (2019).
[13] M. Ezawa, Phys. Rev. B 98, 201402(R) (2018).
[14] T. Hofmann, T. Helbig, C. H. Lee, M. Greiter, R. Thomale, Phys. Rev. Lett. 122, 247702 (2019).
[15] R. Haenel, T. Branch and M. Franz, Phys. Rev. B 99, 235110 (2019)
[16] M. Ezawa, Phys. Rev. B 99, 201411(R) (2019).
[17] M. Ezawa, cond-arXiv:1904.03823 Phys. Rev. B(R) (2019)
[18] M. Ezawa, Phys. Rev. B 100, 045407 (2019)
[19] J. M. Zeuner, M. C. Rechtsman, Y. Plotnik, Y. Lumer, S. Nolte, M. S. Rudner, M. Segev, and A. Szameit, Phys. Rev. Lett. 115, 040402 (2015).
[20] V. V. Konotop, J. Yang, and D. A. Zezyulin, Rev. Mod. Phys. 88, 035002 (2016).
[21] K. G. Makris, R. El-Ganainy, D. N. Christodoulides, and Z. H. Musslimani, Phys. Rev. Lett. 100, 103904 (2008).
[22] H. Schomerus, Opt. Lett. 38, 1912 (2013).
[23] M. Pan, H. Zhao, P. Miao, S. Longhi, and L. Feng, Nat. Commun. 9, 1308 (2018).
[24] H. Hodaei, A. U Hassan, S. Wittek, H. Garcia-Gracia, R. El-Ganainy, D. N. Christodoulides and M. Khajavikhan, Nature 548, 187 (2017).
[25] T. Liu, Y.-R. Zhang, Q. Ai, Z. Gong, K. Kawabata, M. Ueda, F. Nori, Phys. Rev. Lett. 122, 076801 (2019)
[26] S. C. Zhang and J. Hou, Science 294, 823 (2001)
[27] Y. E. Kraus, Z. Ringel, and O. Zilberberg, Phys. Rev. Lett. 111, 226401 (2013)
[28] O. Zilberberg, S. Huang, J. Guglielmon, M. Wang, K. P. Chen, Y. E. Kraus, and M. C. Rechtsman, Nature 553, 59 (2018).
[29] T. Ozawa, H. M. Price, N. Goldman, O. Zilberberg, and I. Carusotto, Phys. Rev. A 93, 043827 (2016)
[30] X. Zhang, Y. Chen, Y. Wang, J. Y. Lin, N. C. Hu, B. Guan, C. H. Lee, cond-mat/arXiv:1710.08385
[31] H. M. Price, O. Zilberberg, T. Ozawa, I. Carusotto, and N. Goldman, Phys. Rev. Lett. 115, 195303 (2015)
[32] M. Lohse, C. Schweizer, H. M. Price, O. Zilberberg and I. Bloch, Nature 553, 55 (2018).
[33] I. Petrides, H. M. Price, and O. Zilberberg, Phys. Rev. B 98, 125431 (2018)
[34] C. H. Lee, Y. Wang, Y. Chen and X. Zhang, Phys. Rev. B 98 (9), 094434 (2018)
[35] M. F. L. Golterman, K. Jansen and D. B. Kaplan, Phys. Lett. B 301, 219 (1993)
[36] X.-L. Qi, T. L. Hughes and S.-C. Zhang, Phys. Rev. B 78, 195424 (2008)
[37] H. Shen, B. Zhen and L. Fu Phys. Rev. Lett. 120, 146402 (2018).
[38] K. Kawabata, K. Shiozaki, M. Ueda, M. Sato, cond-mat/arXiv:1812.09133.
[39] A. P. Schnyder, S. Ryu, A. Furusaki, A. W. W. Ludwig, Phys. Rev. B 78, 195125 (2008)
[40] S. Ryu, A. P Schnyder, A. Furusaki and A. W. W. Ludwig, New J. Phys. 12 065010 (2010)
[41] K. Esaki, M. Sato, K. Hasebe, and M. Kohmoto, Phys. Rev. B 84, 205128 (2011).
[42] S. Yao, F. Song and Z. Wang, Phys. Rev. Lett. 121, 136802 (2018).
[43] F. K. Kunst, E. Edvardsson, J. C. Budich and E. J. Bergholtz, Phys. Rev. Lett. 121, 026808 (2018).
[44] K. Kawabata, K. Shiozaki and M. Ueda, Phys. Rev. B 98, 165148 (2018)
[45] Timothy M. Philip, Mark R. Hirsbrunner, and Matthew J. Gilbert, Phys. Rev. B 98, 155430 (2018)
[46] Y. Chen and H. Zhai, Phys. Rev. B 98, 245130 (2018).
[47] B. Zhu, R. Lu and S. Chen, Phys. Rev. A 89, 062102 (2014).
[48] C. Yin, H. Jiang, L. Li, Rong Lu and S. Chen, Phys. Rev. A 97, 052115 (2018).
[49] S. Lieu, Phys. Rev. B 97, 045106 (2018).
[50] R. Jackiw and C. Rebbi, Phys. Rev. D 13, 3398 (1976)
[51] See Supplemental Material at [xxx] for an explicit form of the circuit Laplacian.